VARIATIONS IN LUNAR ELASTIC THICKNESS FROM SPECTRAL ADMITTANCE ANALYSIS AND SYNTHETIC NOISE TESTS. R.E. Maxwell[1], F. Nimmo[1]. [1]Dept. of Earth and Planetary Sciences, University of California Santa Cruz, Santa Cruz, CA.

Introduction: One way to infer the rate of cooling on the Moon is by measuring the elastic thickness (T_e) [1, e.g.], which is understood to be the minimum elastic thickness since the time of load emplacement. Values of T_e provide an estimate for the thermal gradient at the time of loading. Maps of the variations of T_e show where or when the Moon experienced faster cooling and can place constraints on cooling models.

Previous authors have mapped variations in the lunar T_e [2-3] but paid rather little attention to the uncertainty in these estimates outside of calculating misfits. Our study focuses on estimating uncertainty using synthetic admittance spectra to determine the effect noise has on inverting for T_e.

In this study, we 1) find the best fit T_e values for localized areas using a Markov chain Monte Carlo method in order to map lunar T_e variations and 2) lay the groundwork for determining the uncertainty of the values by creating synthetic admittance and coherence spectra based on actual topography and theoretical T_e values. Combining these two tasks will allow us to determine the uncertainty of our variability map.

Methods: Here we work in the spectral domain and use admittance techniques to find T_e. An admittance spectrum is the ratio of gravity and topography, and the wavelength at which long-wavelength isostatic support transitions to short-wavelength flexural support provides an estimate for T_e [2, 4-5 e.g.]. In our analysis, we replace topography with gravity-from-topography, sometimes called the Bouguer anomaly, because lunar topography is sufficiently rugged that the lunar gravity is not well approximated as a thin sheet [6]. The resulting admittance is now unitless, meaning it will trend toward a value of 1 at higher spherical harmonic degrees.

We use GRAIL and LOLA data [7-9] for our gravity and gravity-from-topography data. We find the best-fit T_e model based on the real localized free air admittance analysis (Fig. 1) using a Markov chain Monte Carlo simulation. We assume only top loading and currently only fit the admittance spectra, but future work will include also fitting the coherence spectra. This inversion is done for all areas on the Moon in order to map the variations in T_e (Fig. 2), though we note that some areas (such as mascons) will not produce credible answers with this type of analysis.

In spectral analyses, there is a tradeoff between spectral and spatial resolution [10]. Larger windows include longer wavelength data but at the expense of spatial resolution while smaller windows increase spatial resolution but disregard wavelength data larger than the window. We choose a window radius of 35° with a window spacing of 15° such that windows will overlap.

To determine the effect of noise on recovering a known T_e, we make use of synthetic admittance spectra and random gaussian noise to the level expected for each admittance spectrum. We create synthetic gravity datasets by multiplying a model admittance with the gravity-from-topography dataset. A localized admittance spectrum is then derived from windowed gravity-from-topography and synthetic gravity in order to determine the localized admittance. We compare the calculated T_e from this admittance spectrum with spectra generated by adding noise to the gravity coefficients, where noise is randomly chosen from a gaussian distribution with a standard deviation equal to the error estimated for each coefficient (eq. 1, below). This is repeated 30 times (Fig. 3).

Results: We map the best-fit T_e values (Fig. 2, bottom). Our results are comparable with the map produced by [2], only different by ~5-10 km in a few areas. [3] found T_e values in five locations, and our values match only two locations well, one location moderately well, and our values do not match the remaining two locations.

Areas where admittance values are negative will not produce meaningful T_e values if only surface loading is assumed. Such areas include the lunar maria (where the surface layer has a greater density than the crust beneath) and mascons (where there is negative topography with positive Bouguer gravity). Correlation values in these regions are also negative, which provides an indication of where we can apply our analyses. We map the averaged correlation values from l = 20-30 (Fig. 2, top), where the flexural transition is expected. For now, we choose a somewhat

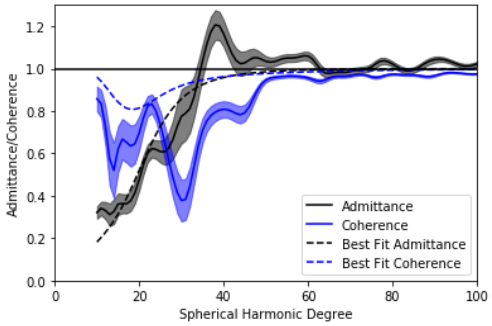

Figure 1. Localized admittance and coherence spectra from 0°N, 180°E compared with spectra for the best-fit T_e value from spherical harmonic degrees 9-100. We use a simple cosine taper given by $\cos(\pi\theta/2\theta_0)$ for $\theta < \theta_0$, where θ_0 =35° is the window radius and θ is the angular distance from the center of the window.

arbitrary cutoff of +0.5 (black lines, Fig. 2) to determine in which regions our analysis cannot be trusted but will explore windows that follow geologic boundaries in the future.

We performed our synthetic tests on two locations as a proof of concept: one where the root mean square (RMS) difference between the real and model admittance spectra is low (good fit) and one where it is high (Table 1).

Discussion: Uncertainty depends on the amount of noise added to the synthetic spherical harmonic coefficients C_{lm}, S_{lm}. We base our estimates of the noise on the measured coherence γ^2 using the equation:

$$\Delta C_{lm} = 1.96\, C_{lm}\, ([\gamma_l^{-2}-1]/[2l+1])^{1/2} \quad (1)$$

where 1.96 is from [11]. ΔS_{lm} is similarly calculated.

RMS values for the synthetic data continue to remain low for the 0°N 180°E noise-added cases (Table 1), suggesting the results are reliable. RMS values for the 45°N 45°E case remain high, suggesting that the best-fit solution does not do a good job of explaining the observations. The standard deviation of the recovered T_e values for the "good" fit case (11.5 km) is higher than the formal standard deviation (2 km) found from the MCMC solution using the real data. We regard the former as a more realistic estimate of the true uncertainty in the T_e value derived.

Conclusions and Next Steps: We have shown preliminary work that will allow us to determine the uncertainty in T_e for each location on the Moon where free air admittance analyses are reasonable. In the future, we will 1) include coherence and subsurface loading in our MCMC approach, 2) explore various tapers and windows that allow us to avoid the lunar maria and mascons, and 3) refine our uncertainty estimation process to ensure we are characterizing the model appropriately.

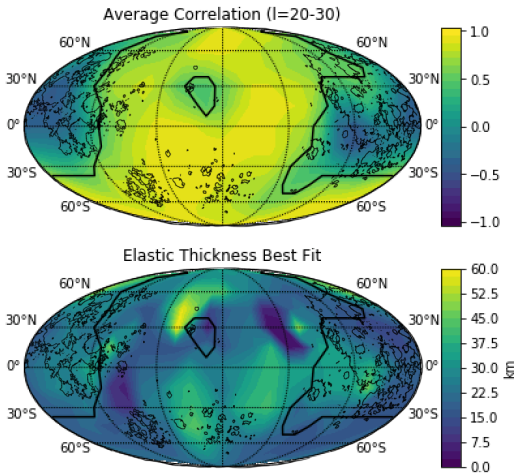

Figure 2. Preliminary map of (top) average correlation (l=20-30) and (bottom) T_e assuming surface loading and using localized admittance spectra with windows of radius 35° and window spacing of 15°. We use a crustal thickness of 30km [11] and crustal density of 2550 kg m^{-3} [13]. Maps are centered on 180° E Longitude. The thick black lines indicate where average correlation is greater than +0.5 and thin black lines show the outline of the mare.

	0°N 180°E	45°N 45°E
RMS Z	0.080	0.298
Synthetic T_e	20 km	5 km
Mean recovered T_e	23.4 km	7.0 km
σ of recovered T_e	11.5 km	3.5 km
Mean RMS of synthetic best-fit Z	0.108	0.303

Table 1. Comparison of a "good" fit (0°N 180°E) versus a "bad" fit (45°N 45°E). The first row shows the RMS of the best-fit solution using the real data. The second row shows the T_e used to make the synthetic data. The following rows describe the results from the 30 noise-added synthetic cases (Fig. 3). Z = admittance; σ = standard deviation.

Acknowledgements: Some portions of the work were supported by NASA grant 80NSSC20K1426.

References: [1] McGovern, P. J., et al. (2002). *JGR:P*, *107*, E12. [2] Audet, P. (2014). *PEPI*, *226*, 48-82. [3] Zhong, Z., et al. (2014). *Adv. Space Res., 54*, 770-779. [4] Forsyth, D.W. (1985). *JGR*, *90*, 12623. [5] McKenzie, D. (1994). *Icarus, 112*, 55-88. [6] Wieczorek, M. A. and R. J. Phillips (1998). *JGR:P, 103.E1*, 1715-1724. [7] Zuber, M.T., et al. (2013). *Science*, *339,*668-671. [8] Lemoine, F.G., et al. (2014). *GRL, 41*, 3382-3389. [9] Smith, D.E., et al. (2010) *Space Sci. Rev., 150*, 209-241. [10] Wieczorek, M.A. and F. J. Simons (2005). *Geophys. J. Int. 162.3*, 655-675. [11] Munk, W.H., & Cartwright, D.E. (1966). *Phil. Trans. R. Soc. Lond. A, 259*, 533-581. [12] Wieczorek, M.A., et al. (2013). *Science, 339*, 671-675. [13] Besserer, J., et al. (2014). *GRL, 41*, 5771-5777.

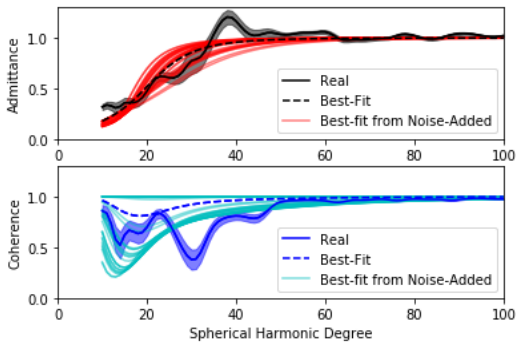

Figure 3. Comparison of admittance and coherence spectra for 0°N 180°E. Solid lines represent real data with transparencies representing error. Dashed lines show best-fit from MCMC inversions. Red/cyan lines show best-fit solutions from inversions on noise-added synthetic gravity data.